

# Programming active metamaterials using topological defects

D. J. G. Pearce,<sup>1,2,3</sup> S. Gat,<sup>4</sup> G. Livne,<sup>4</sup> A. Bernheim-Groswasser,<sup>4</sup> and K. Kruse<sup>1,2,3</sup>

<sup>1</sup>*Dept. of Theoretical Physics, University of Geneva, Switzerland*

<sup>2</sup>*Dept. of Biochemistry, University of Geneva, Switzerland*

<sup>3</sup>*NCCR for Chemical Biology, University of Geneva, Switzerland*

<sup>4</sup>*Dept. of Chemical Engineering, Ben-Gurion University, Israel*

Active metamaterials are able to modify their own shape, providing an exciting range of potential applications. Typically, an active metamaterial contains components able to generate force dipoles, the arrangement of which determines its macroscopic behaviour. In order to fully harness the power of these materials, we must understand how macroscopic morphological changes are determined by the specific orientations and positions of the active components. We show that by imposing topological defects in the arrangements of the force generating components, a thin active sheet is able to realise a range of morphologies. By changing the slope angle, a single spiral defect can lead to positive, negative or zero local Gaussian curvature. In addition, we predict a morphological transition that is controlled by the thickness of the sheet. As a proof of principle, we confirm the existence of this transition by performing an experiment on reconstituted actomyosin gels. Finally, we apply our theoretical analysis to surfaces with different topology. These principles can be applied in the design of programmable active mechanical metamaterials that form the basis for autonomous soft robots.

Metamaterials have unusual properties that are derived from the arrangement of their elementary building blocks rather than their composition [1]. For example, mechanical metamaterials can have negative Poisson ratio [2], vanishing shear modulus [3–5], or negative compressibility [6, 7]. These properties are typically designed into the material and characterise its response to external influence. Programmable mechanical metamaterials include tunable parameters which can be used to directly affect the structure of the elementary building blocks to force the material into a specific response [8].

Active mechanical metamaterials are able to actuate themselves by the inclusion of stress generating components that are driven by some local energy source [9]. By combining the concepts of active and programmable mechanical metamaterials it is possible to design self actuated materials that reproducibly modify themselves. Man-made examples of such materials, often referred to as soft robotics, are scarce because of the tremendous engineering and design challenges. Fortunately, there is a vast array of biological examples from which we can learn key design principles [10].

Developmental biology provides an abundance of examples to learn from. Indeed, as an organism develops, it transitions from a formless mass into its final well defined structure. This transition is driven by internally generated stress and must be highly reproducible. Prominent examples are gastrulation by which a sphere invaginates to form a multilayered structure; the complex folded patterns displayed on the surface of many leaves; the regeneration of the freshwater polyp hydra from a homogenised collection of cells.

In animal systems morphological changes are driven by the actin cytoskeleton, consisting of actin filaments, the molecular motor myosin and other accessory proteins. These components can be extracted, purified and studied in well controlled environments [11, 12]. In particu-

lar elastic acto-myosin gels have been observed to spontaneously buckle upon contraction [13]. Due to the filamentous nature of the actin, which can be associated with a well defined orientation, actomyosin gels can exhibit macroscopic orientational order.

This subcellular order can extend over tissue length-scales [14, 15]. Orientational order fields often exhibit topological defects [16]. These are points at which the orientation cannot be well defined, for example at the centre of a vortex. Topological defects in active materials can focus stress [17, 18] and play a role in processes relevant for organismal development [19–22].

In this paper we shall explore the equilibrium shapes of active elastic thin sheets that contain topological defects. In contrast to many previous theoretical treatments of active surfaces [23–25] we consider the case in which active stresses modify the reference state of an elastic material [26]. This approach allows us to capture patterns of strain that cannot be achieved through external forces.

In the present work we show that topological defects in active elastic sheets can induce spontaneous buckling. The buckled sheets can have positive or negative Gaussian curvature depending on details of the defect and the nature of the active strain. We do this first using an agent based approach which we then coarse grain to a continuum description for active elastic sheets. In this way we identify two possible competing sources of bending, strain driven and spontaneous, with their relative importance being mediated by the thickness of the sheet. This allows us to identify a geometry controlled transition between positive and negative Gaussian curvature sheets. We illustrate this finding with experimental observations on reconstituted actomyosin gels. Finally we demonstrate the applicability of these methods to closed surfaces. Together our results shed light on the development of curved morphologies in developmental biology while also pointing to new opportunities for generating

programmable active metamaterials.

Let's consider an isotropic elastic material with embedded active components able to change the reference state. This change leads to a strain which can result in large scale deformations. We assume there is no background substrate or field to push against, therefore these active components lead to a local expansion or contraction. We consider the case where these local expansions or contractions can be anisotropic. We describe the material as a continuum. The anisotropy of the local expansions and contractions is captured by the coarse grained orientation  $\hat{p}$ , which describes the orientation of principal change. This must be coupled with an order parameter,  $S$ , which describes the local degree of alignment in the active components.

To study the effects of topological defects in the orientation field, we consider originally flat discs with rotational symmetry and symmetry about their mid-plane. These discs are sufficiently thin such that all expansions or contractions are within the plane of the disc, which is homogenous over its height. Consequently we write

$$\hat{p} = \cos(\phi)\hat{e}_r + \sin(\phi)\hat{e}_\theta, \quad (1)$$

where we have employed the orthonormal cylindrical basis  $(\hat{e}_r, \hat{e}_\theta, \hat{e}_z)$ . Furthermore,  $\phi$  is the angle between the average orientation of anisotropic expansion or contraction and the radial direction. We consider the case where  $\phi$  is independent of  $r$ , which dictates the existence of a topological defect at the centre of the disc where the orientation is not well defined. This defect, with topological charge  $+1$ [27], has a characteristic shape which depends on the slope angle  $\phi$ , resulting in either a vortex ( $|\phi| = \pi/2$ ), an aster ( $\phi = 0$ ) or a spiral ( $0 < |\phi| < \pi/2$ ), see SI Fig. S1. As a consequence of the defect  $S$  vanishes at the centre of the disc. We consider the case where  $S$  depends monotonically on  $r$  with  $S(0) = 0$ . We scale the local changes such that  $S(R) = 1$  where  $R$  is the radius of the disc.

We want to study the steady state shapes of such discs in the presence of activity. To this end we subdivide the volume of the disk into a Voronoi tessellation. The corresponding Delaunay Triangulation describes a network connecting the centres of each Voronoi cell. We approximate the stress through each face of a Voronoi cell by springs along the edges of the Delaunay network. To incorporate the active expansions and contractions, we modify the rest length of the spring,  $i$ , according to

$$l_i = l_i^{(0)} \zeta \sqrt{1 + \xi S(r_i) + \lambda S(r_i)(\hat{p} \cdot \hat{l}_i)^2}, \quad (2)$$

where  $l_i^{(0)}$  is the rest length of spring  $i$ , with orientation  $\hat{l}_i$  and midpoint position  $r_i$ , in the absence of activity. We consider all springs to have the same spring constant which we set to unity,  $k = 1$ , and evolve the system according to an over-damped Langevin Equation. The parameters  $\zeta$ ,  $\xi$  and  $\lambda$  are the global, differential isotropic and differential anisotropic expansion or contraction coefficients, respectively. These coefficients could be time

dependent, to reflect a constantly changing active strain, however in the current work we focus on steady states of the gel. Since  $\zeta$  only contributes a global rescaling of the material, we set it to unity in this study.

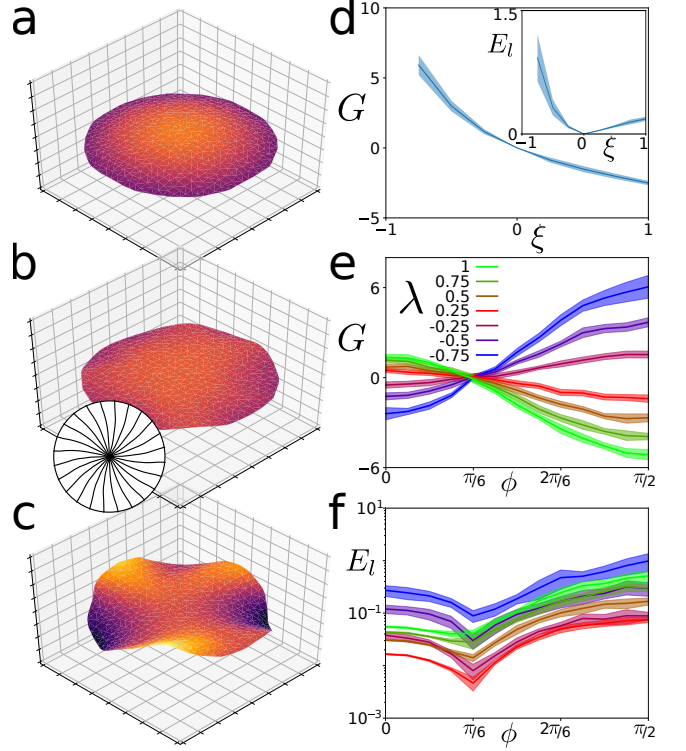


FIG. 1. (a-c) Final surfaces for active expansion ( $\lambda > 0$ ) for an (a) aster ( $\phi = 0$ ), (b) spiral ( $\phi = \pi/6$ ) and (c) vortex ( $\phi = \pi/2$ ) topological defect. (inset b) Final position of initially straight lines for a spiral with  $\phi = \pi/6$ . (d) Integrated Gaussian curvature as a function of isotropic stress. (inset) Stored elastic energy of the surface for varying isotropic stress. (e) Integrated Gaussian curvature for varying anisotropic stress and defect slope angle. (f) Stored elastic energy of the final surface for varying anisotropic stress and slope angle.

Depending on the signs of  $\xi$  and  $\lambda$  the edge of the gel will contract or expand relative to the centre. By adjusting the values of  $\xi$ ,  $\lambda$  and  $\phi$  it is possible to achieve a range of surfaces from domes, to twisted flat sheets, to saddles, see Fig. 1a-c and SI Fig. S2.

In order to quantify these shapes we introduce the integrated Gaussian curvature,  $G = \int_A K$ ; a dimensionless quantity that is negative for saddle shapes, positive for dome shapes and zero for flat discs. We first examine the effects of purely isotropic contraction and expansion,  $\lambda = 0$ . In this case  $G$  changes sign with  $\xi$  which corresponds to a transition from a saddle like surface to a dome, see Fig. 1d.

In the final state of the sheet not all springs of the network are able to relax, hence it stores elastic energy and is in a state of self stress. The total elastic energy stored

in the sheet is given by  $E_l = \frac{1}{2} \sum_i (l_i - x_i)^2$ , where  $x_i$  and  $l_i$  are the length and rest length of spring  $i$ , respectively. The stored elastic energy increases as  $\xi$  deviates from zero, see Fig. 1d(inset).

For purely anisotropic expansions and contractions,  $\xi = 0$ , the value of  $G$  for the final shape of the surface is set by a combination of the sign of the anisotropic stress  $\lambda$  and the slope angle of the topological defect  $\phi$ , see Fig. 1e. This varies monotonically with  $\phi$  with the sign of the gradient being opposite to the sign of  $\lambda$ . Note that,  $G$  passes through zero at  $\phi = \pi/6$  for all values of  $\lambda$ , such that  $\text{sign}(G) = \text{sign}(\pi/6 - |\phi|) \times \text{sign}(\lambda)$ .

When the defect is a spiral the surface exhibits a twisted in plane strain; this can be seen by the final position of initially straight lines, see Fig. 1b(inset). The chirality of this twist reflects the chirality of the initial spiral defect and the sign of  $\lambda$ , see SI. The stored elastic energy has a minimum at this point. This indicates that when  $\phi = \pi/6$  almost the entire strain can be relaxed without inducing integrated Gaussian curvature, see Fig. 1f.

We can describe these thin elastic sheets by their mid-plane  $R(u^1, u^2)$  where  $u^\alpha$ ,  $\alpha = 1, 2$ , are coordinates parametrising the surface. To lowest order in the deformations, the corresponding energy of a surface with thickness  $h$  is given by

$$E = \int_A dA \mathcal{A}^{\alpha\beta\gamma\delta} \left[ \frac{h}{2} u_{\alpha\beta} u_{\gamma\delta} + \frac{h^3}{24} b_{\alpha\beta} b_{\gamma\delta} \right]. \quad (3)$$

Here  $u_{\alpha\beta} = (g_{\alpha\beta} - \bar{g}_{\alpha\beta})/2$  is the two dimensional strain tensor,  $g_{\alpha\beta}$  is the 2D metric tensor and  $\bar{g}_{\alpha\beta}$  is the 2D reference metric. Furthermore,  $b_{\alpha\beta}$  are the components of the second fundamental form and  $dA$  is the area element of the deformed surface. The elastic tensor for an isotropic elastic material is given by  $\mathcal{A}^{\alpha\beta\gamma\delta} = \frac{Y}{1+\nu} \left[ \frac{\nu}{1-\nu} \bar{g}^{\alpha\beta} \bar{g}^{\gamma\delta} + \bar{g}^{\alpha\gamma} \bar{g}^{\beta\delta} \right]$ , with  $Y$  the Young's modulus and  $\nu$  the Poisson ratio.

The elastic energy has two key contributions. The first is the strain energy, associated with stretching the material away from the shape defined by the reference metric. If we define  $u_i^j = \bar{g}^{jk} u_{ik}$  we can write the stretching contribution in the form

$$E_s = \frac{h}{2} \int dA \frac{Y}{1+\nu} \left[ \frac{\nu}{1-\nu} u_\alpha^\alpha u_\beta^\beta + u_\alpha^\beta u_\beta^\alpha \right]. \quad (4)$$

The second contribution is associated with the curvature of the surface and can be re-written in a form akin to the Helfrich energy of fluid membranes,

$$E_b = \frac{h^3 Y}{12(1-\nu^2)} \int dA (2(H - H_0)^2 - (1-\nu)K). \quad (5)$$

Here  $H$  and  $K$  are the mean and Gaussian curvatures of the surface, respectively, and  $H_0$  is the spontaneous curvature.

Both of these contributions to the energy penalize deviation from some desired state; in the case of the bending

energy it has the spontaneous curvature,  $H_0$ , and in the case of the strain energy it has the reference metric,  $\bar{g}_{\alpha\beta}$ . As in Eq. 2 we consider the case where the active effects are homogenous over the height of the material and the system is up-down symmetric. As a consequence, the spontaneous curvature must be zero,  $H_0 = 0$ .

As before, we consider a change in the reference state of the system as a function of the lowest order symmetries, the average orientation,  $\hat{p}$ , and the associated order parameter,  $S$ . We write

$$\bar{g}_{\alpha\beta} = \zeta^2 \left[ \bar{g}_{\alpha\beta}^{(0)} (1 + \xi S(r)) + \lambda S(r) p_\alpha p_\beta \right], \quad (6)$$

where  $\bar{g}_{\alpha\beta}^{(0)}$  is the reference metric for the material in the absence of activity. The reference metric given by Eq. 6 gives the same changes in length as those described by Eq. 2, hence we can relate the properties of  $\zeta$ ,  $\xi$  and  $\lambda$  to their previous interpretation and again we take  $\zeta = 1$ . It is worth noting that the reference metric given by Eq. 6 may be non-embeddable, in this case the strain cannot be completely released.

We minimise the elastic energy given by Eq. 3 using a Monte Carlo approach. Again we study initially flat discs with rotational symmetry, thus a single topological defect with charge +1 and slope angle  $\phi$ . The material's reference metric in the absence of activity is given by  $\bar{g}_{rr}^{(0)} = 1$ ,  $\bar{g}_{\theta\theta}^{(0)} = r^2$  and  $\bar{g}_{\theta r}^{(0)} = 0$ . At each step of the minimisation, we apply one of three possible deformations. These are either a Gaussian 'ridge' with an amplitude increasing towards the edge of the disc, a global twist tangentially shearing the edge of the disc relative to the centre, or a local radial stretch or compression in the plane of the disc, see Fig. S3. Combinations of these perturbations can generate the forms observed in the previous section, see Fig. 2a-c and Fig. S4. The dependency of the integrated Gaussian curvature,  $G$ , on  $\lambda$ ,  $\phi$  and  $\xi$  is also consistent with the previous section, see Fig. 2d and S5.

The total stored elastic energy is shown in Fig. 2e. The continuum approach allows us to measure the bend and strain contributions to the elastic energy separately. The active contraction and expansion only contributes to the strain energy. Buckling of the sheet can release some of this energy, storing it as bend energy. We see that these contributions approximately balance in the final state for most scenarios. The only exception being when  $\phi = \pi/6$  and the surface adopts a purely twisted configuration with relatively low strain energy, see Fig. 2e(inset). As in the Voronoi description, at this point the strain energy can be relaxed in plane without inducing integrated Gaussian curvature.

The reference metric is the only quantity that changes as the Gaussian curvature switches from positive to negative. Hence, this transition is controlled by the strain energy. To link the reference metric to the final Gaussian curvature, it is helpful to consider closed loops at constant  $r$ . Using the reference metric its length is given

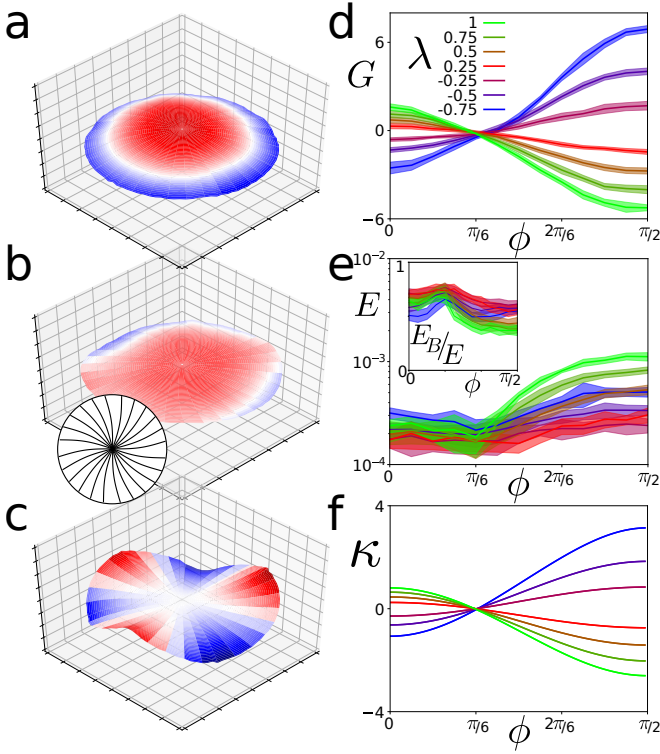


FIG. 2. (a-c) Surfaces minimizing energy Eq. 3 for anisotropic extension ( $\lambda > 0$ ) for an (a) aster ( $\phi = 0$ ), (b) spiral ( $\phi = \pi/6$ ) and (c) vortex ( $\phi = \pi/2$ ) topological defect. (inset b) Final position of initially straight lines for a spiral with  $\phi = \pi/6$ . These are analogous to Figs. 1a-c. (d) Integrated Gaussian curvature for varying anisotropic stress and defect slope angle. This is analogous to Fig. 1e. (e) Stored elastic energy of the final surface for varying anisotropic stress and slope angle. This is analogous to Fig. 1f. (inset) Fraction of elastic energy stored as surface bending. (f)  $\kappa$  as a function of  $\phi$  and  $\lambda$  for the same range of values as Fig. 1e and Fig. 2d.

by

$$p(r) = \int_0^{2\pi} \sqrt{g_{\theta\theta}} d\theta = 2\pi r \sqrt{1 + r^2(\xi + \lambda \sin^2(\phi))}. \quad (7)$$

Its distance from the origin using the same metric is given by

$$\rho(r) = \int_0^r \sqrt{g_{rr}} dr' \quad (8)$$

For a flat reference metric,  $p(r) = 2\pi\rho(r)$ , however for a surface with positive (negative) Gaussian curvature  $p(r) < 2\pi\rho(r)$  ( $p(r) > 2\pi\rho(r)$ ). We now introduce  $\kappa = 1 - p(r)/(2\pi\rho(r))$  which has the same sign as the Gaussian curvature.

For the reference metric given in Eq. 6 we find

$$p(r) = 2\pi r \sqrt{1 + r^2(\xi + \lambda \sin^2(\phi))} \quad (9)$$

and

$$\rho(r) = \frac{\sinh^{-1}(r\sqrt{\beta/2})}{\sqrt{2\beta}} + r \frac{\sqrt{2 + \beta r^2}}{2\sqrt{2}} \quad (10)$$

with  $\beta = 2\xi + \lambda(1 + \cos(2\phi))$ . We calculate  $\kappa$  for a range of  $\lambda$  and  $\phi$ , see Fig. 2f. In particular,  $\kappa = 0$  for  $\phi = \pi/6$  for all  $r$ . At this point the integrated azimuthal and radial strains balance and surface is flat. However, the reference metric still has non-zero off diagonal components,  $\bar{g}_{r\theta} = \lambda S(r) p_r p_\theta$ . Using the double angle formula we write  $p_r p_\theta = \sin(2\phi)/2$ , hence the chirality of the twist changes sign according to  $\text{sign}(\phi) \times \text{sign}(\lambda)$ . This leads to the observed chiral shear for spiral defects, see Figs. 1b(inset) and 2b and SIFig. S6.

These effects can be applied in the design of programmable metamaterials. In order to specify the final shape of the material, one would need to control the properties of the topological defects. These include the slope angle and the degree of isotropic and anisotropic contraction or expansion. As setting these properties can be challenging, we show how the final shape of the sheet can be controlled by a geometrical parameter.

As previously mentioned, the two contributions to the energy penalize deviation from either the reference metric or the spontaneous curvature for the strain and bend energies, respectively. The prefactor of the two contributions to the energy scale with different powers of  $h$ , the thickness of the sheet. If the surface that minimises the bend energy is different from the surface that minimises the strain energy, one might expect a transition between these two states controlled by the thickness.

The minimal surface of the bend energy is flat unless  $H_0 \neq 0$ , in which case it always has positive Gaussian curvature. This is incompatible with any reference metric that leads to negative Gaussian curvature. Since  $E_s/E_b \sim h^2$ , when the surface is sufficiently thin we expect its final shape to be determined by the strain energy, hence having negative Gaussian curvature. However, if  $h$  is sufficiently large we expect the shape to be determined by the bend energy. For  $H_0 \neq 0$  this would result in a surface with positive Gaussian curvature.

We first fix  $H_0 = 1/R$ . In the absence of any active contraction or expansion, this would result in a spherical cap. In order to investigate the transition, we select a reference metric that leads to negative Gaussian curvature. This would be either  $\lambda > 0$  with  $|\phi| > \pi/6$ ,  $\lambda < 0$  with  $|\phi| < \pi/6$ , or  $\xi > 0$ . We observe a transition from negative to positive Gaussian curvature for all three cases as the thickness of the sheet is increased, see Fig. 3a. This transition is associated with an increase in stored elastic energy and a relative decrease in the fraction of energy stored as bend, see Fig. 3b. Confirming our expectation based on the continuum description.

There is no spontaneous curvature in the Voronoi description as defined above. To study the same transition within that framework it is necessary to introduce an additional element. This is possible through the introduction of height dependent contraction or expansion, which



naturally leads to a spontaneous curvature. We write

$$l_i = l_i^{(0)} \zeta (1 + H_0 z_i) \sqrt{1 + \xi S(r_i) + \lambda S(r_i) (\hat{p} \cdot \hat{l}_i)^2}, \quad (11)$$

where  $z_i$  is the initial deviation from the mid-plane of the centre point of spring  $i$ . Using the modified prescription of the activity induced rest length we observe the same transition from negative to positive Gaussian curvature, Fig. 3c, as well as the corresponding increase in stored elastic energy, Fig. 3d. This confirms the proposed mechanism.

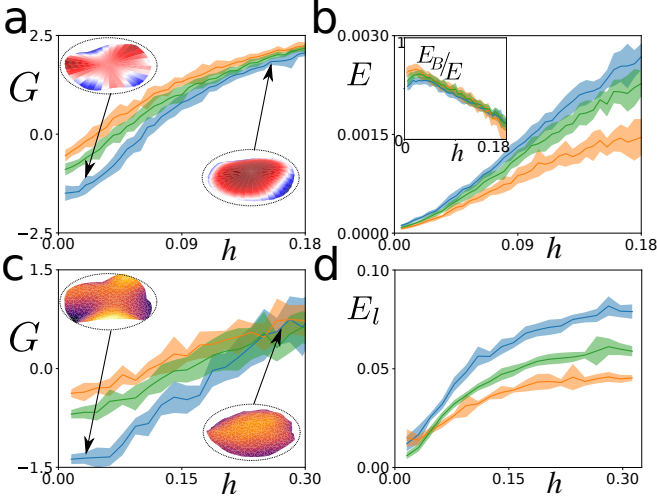


FIG. 3. In all panels  $\lambda = 0.25$ ,  $\phi = \pi/2$  (blue),  $\lambda = -0.25$ ,  $\phi = 0$  (orange), and  $\xi = 0.25$  (green). (a) Integrated Gaussian curvature of minimum energy surfaces as a function of sheet thickness. (inset) Example thin and thick sheets on either side of the transition for  $\lambda = 0.25$ ,  $\phi = \pi/2$ . (b) Minimum energy of the surface for varying thickness. (inset) Fraction of elastic energy stored as surface bending. (c) Integrated Gaussian curvature of final surface using updated dynamics given by Eq. 11. (inset) Example thin and thick sheets on either side of the transition for  $\lambda = 0.25$ ,  $\phi = \pi/2$ . (d) Stored elastic energy,  $E_l$ , of the final surfaces.

The mechanism we have introduced can be applied to any active elastic material in which the components have local orientational order. Gels composed of actin filaments and myosin motors fall into this class of materials. Actin filaments are a biopolymer that forms part of the cytoskeleton and determines, among others, the cell shape. Due to their elongated shape, the actin filaments can be associated with a local orientation.

Myosin is a molecular motor that is able to convert the chemical energy released during the hydrolysis of Adenosine Tri-Phosphate (ATP) into mechanical work. When actin is cross-linked by myosin, there is a resultant active build up of mechanical stresses in the actin filament network. In the presence of an additional actin cross-linker, these stresses can lead to spontaneous contraction of the gel [12].

When contractile actomyosin gels are prepared as a thin sheet, they have been observed to spontaneously

buckle while contracting. This provides an ideal system to illustrate the mechanisms described above. Thus far only negative Gaussian curvature surfaces have been reported[13], see Fig. 4a. From this we can conclude that this buckling is driven by in plane strain since spontaneous curvature can only lead to positive Gaussian curvature.

The gels that were considered were prepared by polymerising actin in the presence of myosin and the strong cross-linker fascin. This yields an elastic contractile actomyosin gel. As the experiments were performed on Earth, up-down symmetry was broken by gravity. This entails an asymmetry in the mechanical properties of the gel. The only element of the proposed theory with the same symmetry is the spontaneous curvature. As per the previous section, if the spontaneous curvature were sufficiently large, this would imply a transition between negative and positive Gaussian curvature as the thickness of the sheet is increased.

We prepared gels of different thickness and allowed them to relax to a mechanically stable state after contraction, which typically took 5 to 15 minutes. Thin sheets displayed saddle like configurations with multiple peaks along the periphery, see Fig. 4a,d,g. As the thickness of the sheet is increased, the number of peaks around the periphery decreases resulting in a normal saddle, see Fig. 4b,e,h. When the sheets are sufficiently thick, they adopt a domed configuration, Fig. 4c,f,i. The domes are all observed to have the same symmetry, being raised in the centre relative to the edge. This is consistent with the bottom surface of the sheet contracting to a higher degree than the top. This supports our statement that gravity breaks the up-down symmetry of the system leading to spontaneous curvature.

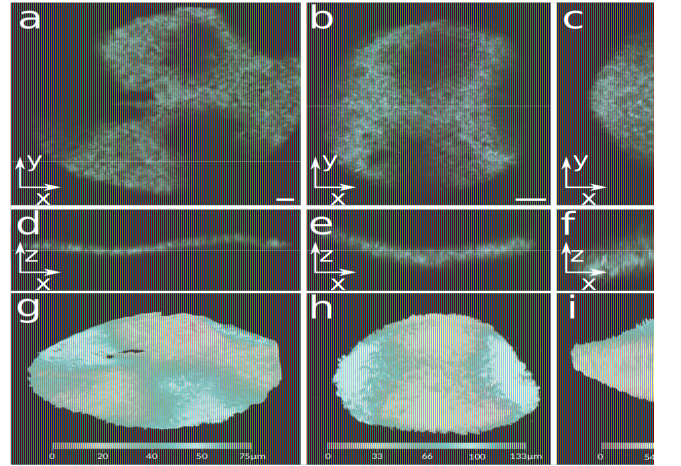


FIG. 4. (a-c) Top and (d-f) side view of actomyosin sheets with increasing thickness. (g-i) Height map of the actomyosin gel after contraction shows a transition from a (g) saddle with three peaks for thin sheets, to a (h) traditional 2 peaked saddle for intermediate thickness, and a (i) domed surface for thick gels.

The theoretical framework introduced is not limited to

initially flat, disc-shaped active elastic materials with +1 topological defects at their centre. Both the agent based and continuum descriptions can be used to describe any thin active elastic with arbitrary initial shape, nematic texture or pattern of local spontaneous curvature. This is demonstrated by studying a spherical nematic shell. Nematic textures on the surface of a sphere are restricted to have net topological charge +2 by the Poincaré-Hopf Theorem, here we choose a nematic texture with two +1 topological defects located at apposite poles.

We fix the angle between the director  $\hat{p}$  and lines of constant azimuth as  $\phi$ ; as before we can identify  $\phi = 0$  with a pair of aster defects,  $|\phi| = \pi/2$  with a pair of vortices, and  $0 < |\phi| < \pi/2$  with a pair of counter rotating spirals, see SI Fig.S7. Similar to the initially flat discs, the final surface depends on the values of  $\phi$ ,  $\xi$  and  $\lambda$ , see Fig. 5.

If we consider the hemisphere containing each defect separately it is possible to infer the final shape of the initially spherical surface. As we know, a contractile vortex or extensile aster defect will tend to increase the Gaussian curvature of the embedding surface. In the case of a sphere, this corresponds to decreasing the radius of curvature for each hemisphere. In the extensile case this leads to an prolate sphere and in the contractile case to the “peanut” shape we observe, see Fig. 5b,c,d. For an extensile vortex or contractile aster, the active stress will reduce the Gaussian curvature. This implies a flattening of the hemisphere, resulting in an oblate spheroid, see Fig. 5a,e. For sufficiently large anisotropic growth each hemisphere adopts a saddle like surface allowing for large regions of negative Gaussian curvature, see Fig. 5f. For spiral topological defects, the surface develops a twist commensurate with the chirality of the defects, see Fig. 5d-f.

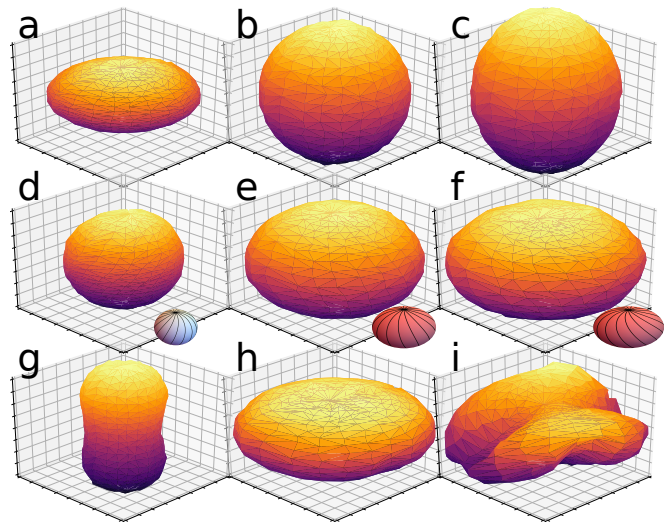


FIG. 5. Example surfaces for an initial spherical sheet with two +1, vortex defects located at opposite poles with (a) contractile ( $\lambda = -0.75$ ) (b) intermediate extensile ( $\lambda = 0.75$ ) and (c) strong extensile active strain ( $\lambda = 1.5$ ).

In this work we have studied the interplay of active stresses and elasticity in thin sheets. We introduce the idea that active stresses can modify the reference metric of a material. This can result in a non-embeddable reference metric, giving patterns of strain which are not achievable through the application of external forces, and can be partially released by the adoption of Gaussian curvature. The corresponding buckling is related to the properties of the new reference metric which we directly relate to the orientation field of stress generating machinery. We have thus far focused on the presence of +1 topological defects within a two dimensional orientation field, however these techniques can be expanded to arbitrary surfaces and nematic textures. Indeed this approach is not limited to thin sheets and can be applied to solid, three-dimensional active elastic materials, with the orientation,  $\hat{p}$ , becoming a full three dimensional vector field.

The placement, charge and slope angle of topological defects within the orientation field can be used to control the folding pattern of the sheets in a predictable manner. Thus by dictating the arrangement of defects, it is possible to design active sheets that evolve into a predetermined shape. Indeed this design principle naturally extends to any specified nematic texture, regardless of the presence of defects. Also, by varying the relative anisotropic and isotropic stresses, it is possible to further expand the space of possible shapes. By exercising time-dependent control over these parameters, one can envision a class of self actuated materials with controllable morphology akin to soft robots.

## ACKNOWLEDGMENTS

We would like to thank Nicholas Ecker for insightful discussions.

- 
- [1] M. Kadic, G. W. Milton, M. van Hecke, and M. Wegener, *Nat Rev Phys* **1**, 198 (2019).
  - [2] R. Lakes, *Science* **235**, 1038 (1987).
  - [3] G. W. Milton, *Journal of the Mechanics and Physics of Solids* **40**, 1105 (1992).
  - [4] M. Kadic, T. Bueckmann, N. Stenger, M. Thiel, and M. Wegener, *Applied Physics Letters* **100**, 191901 (2012).
  - [5] T. Bueckmann, M. Thiel, M. Kadic, R. Schittny, and M. Wegener, *Nature Communications* **5**, 4130 (2014).
  - [6] R. S. Lakes, T. Lee, A. Bersie, and Y. C. Wang, *Nature* **410**, 565 (2001).
  - [7] Z. G. Nicolaou and A. E. Motter, *Nat Mater* **11**, 608 (2012).
  - [8] B. Florijn, C. Coulais, and M. van Hecke, *Phys. Rev. Lett.* **113**, 175503 (2014).
  - [9] A. P. Browning, F. G. Woodhouse, and M. J. Simpson, *Proceedings of the Royal Society A: Mathematical, Physical and Engineering Sciences* **475**, 20190146 (2019).
  - [10] A. Bernheim-Groswasser, N. S. Gov, S. A. Safran, and S. Tzlil, *Adv. Mater.* **30**, 1707028 (2018).
  - [11] A. P. Liu and D. A. Fletcher, *Nat Rev Mol Cell Bio* **10**, 644 (2009).
  - [12] Y. Ideses, A. Sonn-Segev, Y. Roichman, and A. Bernheim-Groswasser, *Soft Matter* **9**, 7127 (2013).
  - [13] Y. Ideses, V. Erukhimovitch, R. Brand, D. Jourdain, J. S. Hernandez, U. R. Gabinet, S. A. Safran, K. Kruse, and A. Bernheim-Groswasser, *Nature Communications* **9**, 1 (2018).
  - [14] H. Gruler, U. Dewald, and M. Eberhardt, *Eur. Phys. J. B* **11**, 187 (1999).
  - [15] G. Duclos, S. Garcia, H. G. Yevick, and P. Silberzan, *Soft Matter* **10**, 2346 (2014).
  - [16] P. G. de Gennes and J. Prost, *The Physics of Liquid Crystals*, 2nd ed., International Series of Monographs on Physics (Oxford University Press, Oxford, 2002).
  - [17] C. Blanch-Mercader, P. Guillamat, A. Roux, and K. Kruse, *arXiv*, 2006.0157 (2020).
  - [18] C. Blanch-Mercader, P. Guillamat, A. Roux, and K. Kruse, *arXiv*, 2006.01725 (2020).
  - [19] T. B. Saw, A. Doostmohammadi, V. Nier, L. Kocgozlu, S. Thampi, Y. Toyama, P. Marcq, C. T. Lim, J. M. Yeomans, and B. Ladoux, *Nature* **544**, 212 (2017).
  - [20] K. Kawaguchi, R. Kageyama, and M. Sano, *Nature* **545**, 327 (2017).
  - [21] Y. Maroudas-Sacks, L. Garion, L. Shani-Zerbib, A. Livshits, E. Braun, and K. Keren, *bioRxiv*, 2020.03.02.972539 (2020).
  - [22] P. Guillamat, C. Blanch-Mercader, K. Kruse, and A. Roux, *bioRxiv* **5**, 2020.06.02.129262 (2020).
  - [23] H. Berthoumieux, J.-L. Maitre, C.-P. Heisenberg, E. K. Paluch, F. Juelicher, and G. Salbreux, *New J Phys* **16**, 065005 (2014).
  - [24] G. Salbreux and F. Juelicher, *Phys Rev E* **96**, 032404 (2017).
  - [25] R. G. Morris and M. Rao, *Phys Rev E* **100**, 775 (2019).
  - [26] D. A. Matoz-Fernandez, F. A. Davidson, N. R. Stanley-Wall, and R. Sknepnek, *Phys. Rev. Research* **2**, 1 (2020).
  - [27] The topological charge of a defect is the number of turns the vector makes when translated along a closed loop encircling the defect core.